Comparison of Thermal Expansion and Oxidation Behavior of Various High-Temperature Coating Materials and Superalloys

J. A. Haynes, B. A. Pint, W. D. Porter and I. G. Wright
Metals and Ceramics Division
Oak Ridge National Laboratory

ABSTRACT

The thermal expansion mismatch between a metallic substrate and its external oxide scale generates a strain on cooling that is a primary cause of spallation of protective oxide scales. This study compares thermal expansion behavior and cyclic oxidation performance of the two major composition classes of high-temperature commercial coatings for protection of single-crystal superalloys. The thermal expansion of cast MCrAlY (M = Ni and/or Co) alloys and cast aluminides (NiAl, (Ni,Pt)Al and Ni_3Al) was measured at temperatures up to 1300°C and compared to that of a single-crystal Ni-base superalloy. The tendency for scale spallation from each alloy was evaluated by cyclic oxidation testing at 1150°C. The coefficients of thermal expansion for the aluminides were lower than those of the MCrAlY-based alloys at all temperatures and scale adherence to the Hf-doped aluminides was generally superior. Scale adherence to the various compositions of MCrAlY-type alloys did not directly correlate to their thermal expansion behavior or substrate strength. For both types of materials, the presence of a reactive element (Y,Hf, etc.) had no detectable effect on thermal expansion but a major effect on scale adherence. There was no obvious influence of Al content on the thermal expansion of   phase Ni-Al compositions. The addition of Pt resulted in a lower average thermal expansion for hyperstoichiometric (Ni,Pt)Al at temperatures above 930°C, but this effect was not observed in hypostoichiometric (Ni,Pt)Al.

INTRODUCTION

The oxidation and corrosion resistance of high-temperature alloys and coatings is dependent on the formation and retention of a thin, dense, continuous external oxide scale, which serves as a diffusion

barrier and prevents rapid oxidation of the underlying metal. Alumina (α-Al_2O_3) is typically the preferred protective scale for applications above 900°C.[1,2] Thus, alumina-forming coatings, including nickel aluminides (NiAl), precious metal-modified aluminides (e.g. (Ni,Pt)Al or (Ni,Pd)Al) and MCrAlX alloys (where M = Ni, Co and/or Fe and X = Y, Hf, Zr and/or Si) are commonly deposited on gas turbine superalloy hardware as oxidation-resistant coatings or as bond coatings for thermal barrier coating (TBC) systems.[2–7]

Adherence of the protective alumina scale to the underlying metal during thermal cycling typically determines the oxidation resistance of a specific alloy or, in the case of a bond coating, the lifetime of a TBC system.[4,6] The growth rate and spallation resistance of alumina scales can vary widely depending on the composition[7,8] of the coating or alloy. Others attribute mechanical properties of the substrate as a key factor in determining oxide adherence.[9,10] The relative importance of each of these factors is not well understood. A better quantification of the phenomena that influence oxide adherence is needed to improve life prediction capabilities and to provide direction for the design of advanced oxidation-resistant alloys and coatings.

Some of the observed variability in protective oxide adherence can be attributed to the detrimental effects of trace impurities, such as sulfur,[11-15] or to the beneficial effects of reactive element (RE) dopants (e.g., Y, Hf or Zr)[7,8,16-20] or precious metal additions (e.g., Pt, Pd or Ir).[7,8,15,21-27] However, even when reactive elements or precious metals are present, there can still be significant variations in scale adherence, depending on the composition and phase content of the alloy. For example, under- or over-doping with a RE may be detrimental.[19] Even when optimally doped with a RE, MCrAlX alloys typically display inferior scale adherence to RE-doped aluminides under thermal cycling conditions,[8,28] although MCrAl-type compositions typically provide superior hot corrosion resistance.[29]

It is well known that residual stresses due to thermal expansion mismatch between metal and oxide play an important role in degrading the adherence of protective alumina.[9,10,30,31] Significant levels of compressive stress are induced during thermal cycling, since the thermal expansion of alumina is less than that of the metallic substrates. Growth stresses in the oxide, as well as plastic deformation of

the alloy at high temperature, can also contribute to the overall residual stress state of the protective scale.

Significant variations in residual stress measurements are reported for alumina scales on various types of substrate [31,32]. These variations are likely due to differences in both the thermal expansion behavior and the high-temperature mechanical properties of the metallic substrates. From this perspective, a comprehensive understanding of the thermal expansion behavior of the various alumina-forming bond coat and substrate combinations would be expected to provide a significant contribution to efforts to model oxidation-dependent degradation processes on advanced coatings. This paper presents thermal expansion data of various Ni-base alumina-formers, specifically cast aluminides, cast MCrAlX alloys and superalloys. The thermal expansion data was compared to cyclic oxidation behavior of each alloy in order to evaluate the relative influences of substrate thermal expansion and alloy composition on oxide scale adherence.

EXPERIMENTAL

Various compositions of MCrAlY, -NiAl, -(Ni,Pt)Al and '-Ni$_3$Al alloys were cast by vacuum induction melting and solidified in a water-chilled copper mold at Oak Ridge National Laboratory (ORNL). Except as noted, these cast alloys were annealed at 1300°C for 4h in quartz ampules. A single-crystal (SX) Ni-base superalloy (René N5) was obtained from Howmet Corporation (Whitehall, MI). The chemical composition of each alloy (Table 1) was measured by inductively coupled plasma analysis (ICP) and combustion analysis of the as-cast materials. All compositions are reported in atom %.

Oxidation coupons (1.5 mm thick, 15 mm diameter) were polished to 0.3 µm alumina and cleaned in acetone and methanol prior to exposure. Cyclic oxidation was performed at 1150°C in dry, flowing oxygen in an automated furnace with specimens attached to alumina rods with Pt-Rh wires. Specimens were inserted into a hot furnace, remained at temperature for 60 minutes and were cooled for 10 min in ambient air to ~30°C between cycles. Specimen mass changes were measured using a Mettler model AG245 balance. Mass changes were corrected for evaporation of the Pt-Rh wires.

The thermal expansion specimens were fabricated via electro-discharge machining (EDM) to a size of either 10 mm or 25 mm length x 3 mm diameter or parallelograms of dimension 2 mm x 3 mm x

10 mm. Alloys that were machined in the as-cast condition were annealed during the course of multiple thermal expansion tests. Expansion measurements were made between room temperature and 1200° or 1300°C while the samples were heated and cooled at a rate of 3°C/min using a Theta Industries (Port Washington, NY) dual push rod differential dilatometer. Data were stored at 30 s intervals. The advantages of such an instrument have been reported by Plummer.[33] The dilatometer was of horizontal configuration with push rods and sample holder constructed of high-density alumina. A tungsten rod with a length of 10 mm was used as the reference material. Differential changes in length between the sample and reference were transmitted to a linear variable differential transformer (LVDT) mounted on an Invar rod, with separate pairs of leaf springs for the coil and core. The leaf springs provided frictionless movement of the LVDT and also maintained a push rod load of 25-30 g on the sample and reference. The LVDT was housed in an enclosure maintained at 40°C by means of water circulated from a constant-temperature bath. A platinum/platinum-10% rhodium type S thermocouple was used to monitor the sample temperature. The accuracy of the expansion measurements was determined to be better than $\pm 2\%$ over the range of 20° to 1450°C by means of verification tests using sapphire and tungsten reference materials heated in the sample and reference positions.

Oxidation of the samples during the dilatometer runs was minimized by evacuating the system using a mechanical vacuum pump followed by backfilling with Ti-gettered He. This process was repeated three times prior to each dilatometer run. During the test a He flow rate of 5 ml/min was maintained at a slight overpressure of 21 kPa (3 psi). Two or three measurements from 20° to 1200°-1300°C were made on most specimens to ensure repeatability and, in selected cases, two separate specimens from each alloy were tested.

RESULTS

Thermal Expansion Measurements

The average coefficient of thermal expansion (CTE) values measured for each alloy over the temperature range 200 - 1300°C are reported in Table 2. The average CTE is commonly used for calculating the cooling stress due to the CTE mismatch in metal-scale systems. Table 2 also lists CTE

data for polycrystalline Al_2O_3 from Reference 34, for comparison to the alloy expansion behavior. Table 3 summarizes for each alloy the number of 1h cycles at 1150°C to zero mass change, the difference in thermal expansion of the alloy and alumina at 1150°C, the RE addition and the estimated equilibrium phase content at 1150°C.[35]

Thermal expansion behavior of MCrAlY alloys

The cast MCrAlY alloys showed significant variation in thermal expansion behavior as a function of composition and temperature. There also were differences in the shapes of their expansion curves. Figure 1 compares average CTE versus temperature for the single-crystal superalloy (nominally along <001>) and the four cast MCrAlY alloys over the temperature range 600 to 1200°C. The single-crystal Ni-base superalloy had the lowest thermal expansion of the MCrAl-based alloys, with no obvious inflections in the expansion curve.

The Ni-7Cr-13Al-Y composition was selected to mimic the Al (6.3 wt..%) and Cr (6.9 wt..%) content of the superalloy (Table 1) for oxidation testing. However, its thermal expansion behavior was quite different from the superalloy both in magnitude and shape of the average CTE curves (Fig. 1). The model low-Cr NiCrAlY had one of the highest average CTE values. The absence of refractory elements in the model alloy resulted in a different phase composition (Table 3) and transformations[35] which contributes to the difference between these alloys.

The NiCo-17Cr-24Al-Y and Ni-20Cr-19Al-Y (Ni-20Cr-10Al-Y in wt%) alloys are common compositions for plasma-sprayed bond coatings [2,3,36-38]. The NiCoCrAlY alloy exhibited the highest average CTE at temperatures below 980°C. The Ni-20Cr-19Al-Y specimen exhibited the lowest CTE of the cast MCrAlY alloys until approximately 650°C. However, this alloy experienced a sharp increase in the slope of the curve from 900 to 1025°C (Fig. 1), indicative of volume expansion due to the $\beta + \gamma'$—$\gamma + \beta$ phase transformation.[35] After this phase transformation, the Ni-20Cr-19Al-Y had the highest total expansion of any alloy above 1000°C. The phase transformation was reversible, based on the shape of the cooling curve and subsequent replicate experiments. The average CTE curves were similar to those previously measured for free-standing vacuum plasma-sprayed Ni-20Cr-19Al-Y,[39] confirming the validity of comparing the thermal expansion of cast MCrAlYs to plasma-sprayed coatings.

5

The Ni-10Cr-19Al-Y alloy (Ni-10Cr-10Al-Y in wt%) was selected as a high-Al, low-Cr composition to avoid the high temperature phase transformation that occurs in Ni-20Cr-19Al.[35] This alloy exhibited the lowest thermal expansion of the cast MCrAlY alloys with a curve shape nearest that of the superalloy.

Thermal Expansion Behavior of Aluminide Alloys

The compositions of the -NiAl alloys were chosen to reflect Al contents on both sides of the stoichiometric composition. Platinum-modified -NiAl compositions also were included in order to investigate whether the beneficial effect of Pt on scale adherence was related to modification of the thermal expansion behavior. Small amounts of Hf were added to most alloys to improve scale adherence during cyclic oxidation testing.

Figure 2 compares the average CTE behavior of the single-crystal Ni-based superalloy to that of three -NiAl alloys and a Ni₃Al cast alloy over the temperature range 600° to 1300°C. The four intermetallic curves were similar and each exhibited a slight increase in slope above ~1000°C. In comparison, the thermal expansion of the Ni-base superalloy was substantially higher than the aluminides above 1000°C. The ' alloy (Ni-25Al+Hf) exhibited the lowest average CTE of all aluminides below 1200°C (Fig. 2). However, its thermal expansion increased rapidly above 1200°C, making it equal to or higher than the -NiAl alloys.

There was no apparent influence of Al or Hf content on -NiAl thermal expansion. The thermal expansion behavior of the three NiAl alloys (Ni-50Al+Hf, Ni-50Al and Ni-40Al) was nearly identical up to 800°C, after which there were minor variations in the curves (Fig. 2). The expansion curve measured for the Ni-50Al alloy in this study was nearly identical to those measured previously [40,41] up to 1000°C (the temperature limit of the previous studies). The limited influence of Al content on the Ni-Al thermal expansion behavior also was in agreement with previous work.[40]

The addition of 2.3 at% (10 wt%) Pt to hyperstoichiometric Ni-52Al alloys resulted in a lower average thermal expansion at higher temperatures, compared to NiAl or Ni₃Al (Fig. 3). Both the NiPt-52Al and NiPt-52Al+Hf had very similar thermal expansion curves, with the exception of a slight downward inflection in the Hf-containing (Ni,Pt)Al at ~950°C. Unlike the curves of the NiAl, NiAl+Hf

and Ni_3Al+Hf alloys, there was no rapid increase in slope of these hyperstoichiometric Pt-containing intermetallics above 950°C (Fig. 2). These results were consistent during duplicate tests of each type specimen.

A similar effect did not occur when Pt was added to hypostoichiometric -NiAl. The addition of 2.5 and 5.6% Pt to Ni-49.7% Al and Ni-39Al, respectively, did not result in a lower thermal expansion relative to Ni-50.1Al, Figure 3. The thermal expansions of these two alloys were actually slightly higher than those of the NiAl alloys (Fig. 3) above 800°C. Thus, the presence of Pt did not reduce the thermal expansion of -NiAl with Al contents similar to that of single phase aluminide bond coatings (40 at%).[13,15,24-26]

Cyclic Oxidation Behavior

Figures 4, 5 and 6 show the 1150°C cyclic oxidation curves of the various MCrAlY alloys, NiAl and Ni_3Al intermetallics, and the Pt-modified intermetallics, respectively. Each of these alloys formed Al_2O_3 scales during oxidation at 1150°C, although the MCrAlY and Ni_3Al alloys also formed smaller amounts of Ni-rich and/or Cr-rich spinels. Specimen mass losses indicate scale spallation.

Cyclic Oxidation of MCrAlY Alloys

There were dramatic differences in the scale spallation behavior of the four MCrAlY alloys and the SX superalloy, René N5. The superalloy had the best scale adherence of all the MCrAl-based alloys (Fig. 4), as well as the lowest CTE at 1150°C. The Ni-20Cr-19Al-Y, which had the highest CTE at 1150°C, also had the worst oxide adherence of the NiCrAl alloys. However, the Ni-7Cr-13Al-Y showed the best oxide adherence of the cast MCrAlYs, although it had an intermediate CTE value as compared to the other MCrAlY compositions.

In order to demonstrate the importance of the reactive element addition to scale adherence, Fig. 4 also includes the 1150°C cyclic oxidation behavior of Ni-7Cr-13Al with no Y addition. This alloy exhibited very poor scale adherence with massive spallation initiating in less than 20 cycles. By comparison, the Y-doped Ni-7Cr-13Al did not begin to experience significant spallation until ~600 cycles, and the superalloy (which contained Hf and Y) maintained an adherent scale to greater than 900 cycles.

Cyclic Oxidation of Aluminide Alloys

Figure 5 compares the 1150°C cyclic oxidation behavior of the cast β-NiAl and β'-Ni₃Al alloys to that of the superalloy. Two groups of behavior are readily distinguished from Fig. 5. Specimens with a RE addition exhibited superior scale adherence as compared to the un-doped alloys. Comparison of the mass change curves of Ni-50Al and Ni-50Al+Hf alloys in Fig. 5 clearly demonstrates the effectiveness of a RE addition to improve oxide adherence. The cyclic oxidation of the Ni-50Al+Hf (β-phase) alloy was superior to that of the superalloy and the Ni-25Al+Hf (β' phase) alloy. The mass loss of the β' alloy cannot be explained by CTE differences, since its CTE at 1150°C was slightly lower than that of the β alloys (Fig. 2). However, its lower Al content and/or the formation of spinel oxides may play a role.[42] Nevertheless, oxide adherence to the Hf-doped cast aluminides was much better than that of any of the cast NiCrAlY alloys (Fig. 4).

Figure 6 compares cyclic oxidation mass changes of several Pt-modified NiAl alloys. The addition of Pt to both stoichiometric and hyperstoichiometric NiAl significantly improved scale adherence and increased the time required to attain the maximum value in the mass gain curve to ~550 cycles. The oxidation behavior of the Hf-doped NiPt-52Al and NiPt-50Al alloys was nearly identical to that of the Ni-50Al+Hf (Fig. 5), with no evidence of mass loss after 1000 cycles. The rates of mass gain of the un-doped NiPt-52Al and NiPt-50Al alloys were much higher than that of the Hf-doped alloys, suggesting a faster-growing but largely adherent alumina scale.[7,8] Furthermore, the oxidation behavior of NiPt-52Al and NiPt-50Al were nearly identical, suggesting that Al content exerts little influence on oxide adherence in this composition range.

The Al content did play an important role in oxide adherence to some (Ni,Pt)Al compositions. The Ni-5.6Pt-39Al alloy began to show measurable mass loss after only 60 cycles, although it spalled rather slowly out to approximately 600 cycles. By comparison, a near identical composition with no Pt, Ni-40Al, experienced massive spallation after only 40 cycles. A higher-Al, lower-Pt version, Ni-2.4Pt-50Al, did not experience mass losses until after 600 cycles. For both Ni-40Al and -50Al, Pt reduced scale spallation compared to the Pt-free aluminide. However, both alloys with ~40Al showed more scale spallation than the near-stoichiometric aluminides.

DISCUSSION

In evaluating the data presented here, it is important to try to address all of the relevant issues. In general, two groups of alloys were evaluated, MCrAlYs and aluminides. Compared to a SX superalloy, all the MCrAlYs have higher thermal expansion and poorer spallation resistance. In contrast, all the aluminides have lower thermal expansion and, when doped with a RE, all have better spallation resistance. However, trying to draw a direct correlation between CTE and spallation resistance is plagued with problems. The most important of these is that RE additions have the largest effect of any variable on spallation resistance and it appears from this work that RE additions (as expected) have a negligible effect on CTE. Also, while it is straightforward to rank the relative thermal expansion behaviors of these alloys at 1150°C, it is difficult to quantify their spallation resistance. In this case, time to zero mass gain has been adopted for convenience as has been done for lifetime modeling.[43] However, this method requires an estimate for NiAl+Hf and (Ni,Pt)Al+Hf as neither has been observed to reach zero mass gain (ZMG), the former showing minimal spallation after more than 6,000 1h cycles.[44]

Figure 7 compares the thermal expansion mismatch between alloy and alumina at 1150°C and the time to zero mass change for various NiAl and NiCrAl compositions. For Hf-doped aluminides a time of 10,000h has been estimated. In order to illustrate the importance of the RE effect, a few additional alloys have been added or highlighted. As has already been shown, without RE doping, the time to ZMG for NiAl without Hf is only 220h and for undoped Ni-7Cr-13Al, even shorter. Some additional issues are addressed by adding data points for oxide dispersion strengthened (ODS) Ni$_3$Al [42] and a co-doped Ni-20Cr-19Al (with Y and Hf) alloy. Improved spallation resistance has been observed for co-doped alloys by reducing the Y content and adding Hf [45] as is found in René N5 and was suggested for MCrAl bond coats.[46]

With this level of scatter in the data, it is clear that there is no simple correlation between spallation resistance and CTE. However, some specific examples from the current data set appear to illustrate some important issues about the interrelated phenomena of thermal expansion, substrate strength, RE effects and spallation resistance. First, even with an optimized RE addition, Ni-20Cr-19Al+Y/Hf could only achieve a time to ZMG of 625 cycles at 1150°C. This is more than an order of

magnitude worse than Hf-doped NiAl. The CTE mismatch for Ni-20Cr-19Al would appear to be a limiting factor since NiCrAl is quite weak at high temperatures and should accommodate any growth stress or thermal stresses generated in the scale at temperature.[9,10]

Second, it is interesting to consider the case of Hf-doped Ni_3Al compared to the other alloys. Even with a low CTE mismatch and a Hf addition, its time to ZMG was still less than 1000h. This behavior could be attributed to several factors. Ni_3Al has much higher strength than NiAl at these temperatures, and thus could be more prone to spallation because it does not accommodate scale stresses. This hypothesis is supported by the performance of ODS Ni_3Al [42] which has higher creep strength than cast Ni_3Al but a lower number of cycles to ZMG than either Hf-doped NiAl or Ni_3Al. However, the spallation ranking of the Ni_3Al alloys may be skewed by their low Al content. The mass change behavior of Ni_3Al+Hf could be quite different than some of the other alloys. Ni_3Al forms a blue, transient $NiAl_2O_4$ scale followed by an inner alumina scale. On ODS Ni_3Al, this outer scale has been observed to spall and regrow while the underlying alumina remains cracked but essentially adherent.[42] The mass change associated with the growth and spallation of this transient spinel layer could prematurely cause this alloy to reach ZMG. (Similar minor spallation on Hf-doped NiAl might be quickly healed without the formation of a spinel oxide, resulting in negligible mass change.) Thus, Ni_3Al+Hf may be ranked lower in spallation resistance because of its transient oxidation behavior, not because of its alumina scale adhesion. However, a similar argument could be used for the ranking of Ni-7Cr-13Al-Y and the SX superalloy, as both can form transient oxides. This case illustrates the problem of trying to compare the relative scale adhesion of these alloys.

It is clear from the data in Figure 7 that RE doping has a stronger effect on time to ZMG than thermal expansion. If each alloy type had an optimized RE addition, it might be much easier to assess the role of thermal expansion on scale spallation. While Hf-doped NiAl[7,8] and the SX superalloy[47] are thought to be nearly optimized, the various other alloys are not. It is suggested that Ni-7Cr-13Al+Y had a relatively long time to ZMG because of its nearly optimized, low Y level, Table I. In contrast, the higher Y contents of the other MCrAlY alloys correlated with shorter times for these materials. When optimized with both Y and Hf, the time to ZMG of Ni-20Cr-19Al increased by a factor of 5, Figure 7.

Data for alloys with optimized RE additions also might make it easier to assess the effect of substrate strength on scale spallation, especially for the SX superalloy, René N5. From the present data set, it could be concluded that it performed relatively well despite its good creep strength. However, it may be performing much better than some of the other MCrAlY alloys because of its optimized RE addition of both Hf and Y. If RE optimization produced a similar 5X benefit for Ni-10Cr-19Al+Y or NiCoCrAlY, their number of cycles to ZMG would exceed that of the superalloy, even though they have larger CTE mismatches.

One hypothesis is that if the RE addition were optimized for each class of alloys, CTE could then be shown to be the first-order limiting factor for spallation resistance, followed by other factors such as substrate strength. If this hypothesis were correct, then Hf-doped aluminides and the co-doped Ni-20Cr-19Al should set an upper bound of time to ZMG versus CTE mismatch (e.g., the dashed line in Figure 7). Based on this hypothesis, the reason that the superalloy, Ni_3Al+Hf and ODS Ni_3Al do not reach this upper bound is that they have higher creep strength, which decreases their spallation resistance.[9,10]

If one assumes that CTE is not an important factor and only considers creep strength in determining spallation resistance, then the excellent behavior of the Hf-doped aluminides may be explained by their low creep strength relative to the MCrAlY alloys. However, this hypothesis fails to explain why the most creep-resistant alloys, René N5 and Ni_3Al+Hf, outperform weaker NiCrAlY's, even the optimized, co-doped Ni-20Cr-19Al+Y,Hf. These results suggest that substrate creep strength fails to explain the relative spallation resistance of this set of alloys.

Aside from spallation behavior, another general issue to consider is the role of secondary alloy additions in changing the thermal expansion behavior. The reduction in thermal expansion that results from adding >5.5 at% of high atomic number refractory metals (W, Ta, Re, Mo) to the SX superalloy is clearly demonstrated by comparison to the Ni-7Cr-13Al alloy (with the same Al and Cr content as the superalloy). Thermal expansion of the superalloy was further reduced by the higher ' content (' is stabilized by many of the alloying additions in René N5) as compared to the cast MCrAlY alloys.

Considering the role of Pt on thermal expansion, one intriguing result was that the Al-rich (Ni,Pt)Al alloys showed the lowest thermal expansion of any of the alloys tested. Unlike the Pt-free

aluminides, these alloys did not show an accelerated increase in thermal expansion at temperatures over 900°C. Thus, by 1150°C, the Al-rich (Ni,Pt)Al alloys showed significantly lower thermal expansions. These observations can lead to speculation about the possibility of a decrease in the concentration of point defects (especially thermal vacancies) in the alloy with the addition of Pt. A reduction in the number of vacancies could explain the observed reduction in the number and size of interfacial voids with the addition of Pt,[15,24,25] as these voids are thought to form by vacancy coalescence.[48,49] Such a mechanism could explain the improved scale adhesion with the addition of Pt. The shape of the CTE curve for these alloys also could explain observations that Pt additions are more effective at higher temperatures (>1050°C).[15,21,25-27,50,51]

This speculation about the role of Pt must be tempered by the observation that (Ni,Pt)Al alloys with lower Al contents do not show similar low CTE values. Since aluminide bond coatings typically contain Al levels of 40 at.%, the results for the Al-rich alloys appear less relevant to those systems. In the alloys with compositions closer to commercial aluminide bond coats, the lower Al and addition of Pt appeared to have little effect on the thermal expansion compared to near-stoichiometric NiAl.

Most of the discussion has centered on the CTE mismatch between the alloys and alumina as it pertains to thermal strains and scale adhesion. However, another mismatch to consider for a coating system is between the substrate and the coating itself. In this regard, it is interesting that all of the MCrAlY compositions examined have higher thermal expansion than the superalloy. Thus, it would be expected that MCrAlY coatings would be placed in compression by the substrate during heating and, if the stress is relaxing at temperature, would again experience compression during cooling. In contrast, the average CTE curves of the aluminides straddle that of René N5, being lower at higher temperatures. Thus, aluminide bond coatings could be in tension on heating and compression on cooling leading to problems of thermal fatigue. These stresses also may cause some of the surface deformation that has been observed in several studies of laboratory and commercial aluminide bond coatings.[6,50,52]

Summary

1.   The thermal expansion behavior of various MCrAlY, superalloy, Ni_3Al, NiAl and (Ni,Pt)Al castings was measured at temperatures up to 1300°C and the relative scale adherence of each alloy was compared by thermal cycling at 1150°C.

2.   Trends in scale adherence were difficult to correlate with thermal expansion for these alloys because reactive element additions strongly affect scale adherence without changing the thermal expansion.

3.   Scale adherence of the various Hf-doped NiAl alloys was much higher than that of the MCrAlY-type alloys and the Hf-doped NiAl thermal expansion was lower. The thermal expansion behavior of phase Ni-Al was not sensitive to Al or Hf content.

4.   The addition of Pt to Al-rich -NiAl improved scale adherence and clearly reduced thermal expansion, with a lower average thermal expansion occurring at temperatures above 950°C. However, the addition of Pt to stoichiometric or Ni-rich -NiAl improved scale adherence while having little effect on the thermal expansion behavior.

References

1.   Birks, N., Meier, G. H. and Pettit, F. S. *JOM*, **46**(12), 42-46 (1994).
2.   Mévrel, R. *Mater. Sci. Eng.,* **A120**, 13-24 (1989).
3.   Haynes, J. A., Ferber, M. K. and Porter, W. D. *J. Thermal Spray Technol.*, **9**(1), 38-48 (2000).
4.   Maricocchi, A., Bartz, A. and Wortman, D. *J. Thermal Spray Technol.,* **6**(2), 193-198 (1997).
5.   Nicholls, J. R. *JOM*, **52**(1), 28-35 (2000).

6.   Gell, M., Vaidyanathan, K., Barber, B., Cheng, J. and Jordan, E. *Met. Trans.*, **30A**, 427-435 (1999).

7.   Pint, B. A., Wright, I. G., Lee, W. Y., Zhang, Y., Prü ner, K. and Alexander, K. B. *Mater. Sci. Eng.*, **A245**, 201-211 (1998).

8.   Pint, B. A., Haynes, J. A., More, K. L., Wright, I. G. and Leyens, C. In: *Superalloys 2000*. (Eds. T. M. Pollock, R. D. Kissinger, R. R. Bowman, K. A. Green, M. McLean, S. L. Olson and J. J. Schirra) TMS, Warrendale, PA, pp.629-38 (2000).

9.   Evans, H. E., Nicholls, J. R. and Saunders, S. R. J. *Solid State Phenomenon,* **41**, 137-56 (1995).

10. Nicholls, J. R., Evans, H. E. and Saunders, S. R. J. *Mater. High Temp.,* **14**, 5-13 (1997).

11. Smeggil, J. G. *Mater. Sci. Eng.*, **87**, 261-5 (1987).

12. Smialek, J. L., Jayne, D. T., Schaeffer, J. C. and Murphy, W. H. *Thin Solid Films*, **253**, 285-92 (1994).

13. Lee, W. Y., Zhang, Y., Wright, I. G., Pint, B. A. and Liaw, P. K. *Met. Trans.,* **29A**, 833-841 (1998).

14. Sarioglu, C., Stinner, C., Blachere, J. R., Birks, N., Pettit, F. S., Meier, G. H. and Smialek, J. L. In: *Superalloys 1996*. (Eds. R. D. Kissinger, D. J. Deye, D. L. Anton, A. D. Cetel, M. V. Nathal, T. M. Pollock and D. A. Woodford) TMS, Warrendale, PA, pp.71-80 (1996).

15. Haynes, J. A., Zhang, Y., Lee, W. Y., Pint, B. A., Wright, I. G. and Cooley, K. M. In: *Elevated Temperature Coatings: Science and Technology III*, (Eds. J. M. Hampikian and N. B. Dahotre) TMS, Warrendale, PA, pp.185-96 (1998).

16. Strawbridge, A. and Hou, P. Y. *Mater. High Temp.,* **12**, 177-81 (1994).

17. Stringer, J. *Mater. Sci. Eng.,* **A120**, 129-137 (1989).

18. Funkenbusch, A. W., Smeggil, J. G. and Bornstein, N. S. *Met. Trans.,* **16A**, 1164-6 (1985).

19. Pint, B. A. *Oxid. Met.,* **45**, 1-37 (1996).

20. Hou, P. Y. and Smialek, J. L. *Mater. High Temp.,* **17**, 79-85 (2000).

21. Felten, E. J. *Oxid. Met.*, **10**, 23-28 (1976).

22. Felten, E. J. and Pettit, F. S. *Oxid. Met.*, **10**, 189-223 (1976).

23. Farrell, M. S., Boone, D. H. and Streiff, R. *Surf. Coat. Technol.*, **32**, 69-84 (1987).

24. Zhang, Y., Lee, W. Y., Haynes, J. A., Wright, I. G., Pint, B. A., Cooley, K. and Liaw, P. K. *Met. Mater. Trans.,* **30A**, 2679-87 (1999).

25. Zhang, Y., Haynes, J. A., Lee, W. Y., Wright, I. G., Pint, B. A., Cooley, K. M. and Liaw, P. K. *Met. Mater. Trans.*, **32A**, 1727-1741 (2001).

26. Haynes, J. A., More, K. L., Pint, B. A., Wright, I. G., Cooley, K. and Zhang, Y. *Mater. Sci. Forum*, **369-372**, 679-86 (2001).

27. Monceau, D., Bouhanek, K., Peraldi, R., Malie, A., and Pieraggi, B. *J. Mater. Res.,* **15**, 665-675 (2000).

28. Pint, B. A., More, K. L., Tortorelli, P. F. and Wright, I. G. *Mater. High Temp.,* **17**, 165-171 (2000).

29. Leyens, C., Wright, I. G., and Pint, B. A. *Mater. Sci. Forum,* **369-372**, 571-8 (2001).

30. Evans, H. E. *Mater. Sci. Eng.,* **A120**, 139-146 (1989).

31. Sarioglu, C., Schumann, E., Blachere, J. R., Pettit, F. S. and Meier, G. H. *Mater. High Temp.,* **17**, 109-115 (2000).

32. Pint, B. A., More, K. L., Tortorelli, P. F., Porter, W. D. and Wright, I. G. *Mater. Sci. Forum*, **369-372**, 411-8 (2001).

33. Plummer, W. A. In: *International Symposium on Thermal Expansion of Solids*. American Institute of Physics Conference Proceedings, New York (1973) 17.

34. Touloukian, Y. S., Kirby, R. K., Taylor, R. E. and Lee, T. Y. R. In: *Thermophysical Properties of Matter, Volume 13, Thermal Expansion Nonmetallic Solids*. Plenum, New York, NY, p.176 (1977).

35. Merchant, S. M. and Notis, M. R. *Mater. Sci. Eng.,* **66**, 47-60 (1984).

36. Bose, S. and DeMasi-Marcin, J. *J. Thermal Spray Technol.*, **6**(1)**,** 99-104 (1997).

37. Wortman, D. J., Nagaraj, B. A. and Duderstadt, E. C. *Mater. Sci. Eng.,* **A121**, 433-440 (1989).

38. Haynes, J. A., Rigney, E. D., Ferber, M. K. and Porter, W. D. *Surf. Coatings Technol.*, **86-87,** 102-108 (1996).

39. Hillery, R. V., Pilsner, B. H., McKnight, R. L., Cook, T. S. and Hartle, M. S. Thermal Barrier Coating Life Prediction Model Development" Final Report, NASA CR 180807, National Aeronautics and Space Administration, Washington DC, Nov. 1988.

40. Clark, R. W. and Whittenberger, J. D. In: Thermal Expansion – 8. (Ed. T. A. Hahn) Plenum Press, New York, NY, p.189 (1984).

41. Touloukian, Y. S., Kirby, R. K., Taylor, R. E., and Lee, T. Y. In: *Thermophysical Properties of Matter, Vol. 12, Thermal Expansion – Metallic Elements and Alloys*. IFI/Plenum Co., New York, p.438 (1977).

42. Pint, B. A., Garratt-Reed, A. J. and Hobbs, L. W. *Oxid. Metals*, **56**, 121-47 (2001).

43. Smialek, J. L., Nesbitt, J. A, Barrett, C. A. and Lowell, C. E. In: *Cyclic Oxidation of High Temperature Materials*. (Eds. M. Schütze and W. J. Quadakkers) Institute of Materials, London, UK, pp.148-68 (1999).

44. Pint, B. A. and Wright, I. G. for submission to Oxidation of Metals.

45. Pint, B. A. for submission to Journal of the American Ceramic Society.

46. Gupta, D. K. and Duvall, D. S. In: *Superalloys 1984*. (Eds. M. Gell, et al.) TMS, Warrendale, PA, pp.711-20 (1984).

47. Smialek, J. L. and Pint, B. A. *Mater. Sci. Forum*, **369-372**, 459-66 (2001).

48. Hindam, H. M. and Smeltzer, W. W. *J. Electrochem. Soc*. **127**, 1630-1635 (1980).

49. Hutchings, R., Loretto, M. H. and Smallman, R. E. *Metal Science*, **15**, 7- 13 (1981).

50. Haynes, J. A., Zhang, Y., Pint, B. A., More, K. L. and Wright, I. G. *Oxid. Met.*, **58**, 513-544 (2002).

51. Haynes, J. A. *Scripta Mater.,* **44**, 1147-52 (2001).

52. Tolpygo, V. K. and Clarke, D. R. *Acta. Mater.*, **48**, 3283-3293 (2000).

Table 1. Compositions of cast alloys by ICP and combustion analysis (at%)

Alloy	Ni	Pt	Al	Co	Cr	Y	Hf	S	C
Ni10Cr19AlY	70.4		19.4		9.9	0.04		0.0026	0.043
Ni50Al+Hf	49.8		50.1				0.05	#	0.040
NiPt52Al	45.8	2.3	51.8					0.001	#
Ni20Cr19AlY	60.9		19.0		20.0	0.05		0.0008	0.040
Ni50Al	49.9		50.1				#	0.040	
NiCo17Cr14AlY	41.8		23.5	16.9	17.4	0.32	0.07	0.0005	0.040
NiPt52Al+Hf	45.2	2.4	52.2				0.05	#	0.040
Ni7Cr13AlY	80		12.5		7.2	0.012		0.003	0.045
Ni40Al	59.7		40.3				#	0.040	
SX René N5*	64.9		13.9	7.3	7.8	0.003	0.05	0.0007	0.250
Ni25Al+Hf	75.1		24.8				0.06	#	0.041
NiPt50Al+Hf	47.8	2.5	49.7				0.05	0.0004	0.040
NiPt39Al	55.8	5.6	38.7					#	0.027
NiPt-50Al	47.4	2.4	50.2					0.0004	0.04

\# - below ICP detection limit for S of 4ppma and C of 0.04 at%

* René N5 also contained: 2.11 Ta, 1.61 W, 1.02 Re, 0.90 Mo, 0.15 Si, 0.0125 Ti, 0.003 Zr

Table 2. Average Coefficient of Thermal Expansion (ppm/°C)

Nominal Composition (at%)	200°C	600°C	800°C	900°C	1000°C	1100°C	1150°C	1200°C
Al_2O_3[+]	7.5	8.6	9.2	9.4	9.7	10.0	**10.1**	10.3
NiPt52Al+Hf	13.4	14.2	14.5	14.6	14.8	15.0	**15.1**	15.2
NiPt52Al	13.5	14.3	14.6	14.8	14.9	15.1	**15.2**	15.2
Ni40Al	13.8	14.8	15.1	15.3	15.4	15.5	**15.6**	15.7
Ni50Al+Hf	14.0	14.7	14.7	14.9	15.0	15.4	**15.6**	15.9
Ni50Al	13.5	14.5	14.8	15.0	15.3	15.6	**15.8**	15.9
Ni25Al+Hf	13.0	14.1	14.5	14.8	15.1	15.4	**15.6**	15.9
NiPt39Al	13.4	14.6	15.0	15.3	15.6	15.9	**16.0**	16.2
NiPt50Al+Hf	13.6	14.6	14.9	15.1	15.5	15.9	**16.1**	16.4
NiPt35Al+Hf	12.6	14.2	14.7	15.2	15.6	16.1	**16.4**	16.5
superalloy	12.6	13.7	14.4	15.0	15.7	16.6	**17.2**	17.9
NiCrAlY	13.5	14.6	15.2	15.8	16.4	17.2	**17.8**	18.6
NiCo17Cr14AlY	13.7	15.3	17.1	17.9	18.5	18.9	**19.1**	19.5
Ni7Cr13AlY	14.1	15.9	17.0	17.7	18.6	19.2	**19.3**	19.4
Ni20Cr19AlY	13.3	14.6	15.7	16.3	18.9	20.2	**20.3**	20.4

[+] from reference 34

Table 3. Comparison of Number of 1h Cycles to Zero Mass Gain at 1150°C to CTE difference with Al_2O_3 at 1150°C, Alloy RE content and Phase Composition.

Alloy Composition (at.%)	Cycles to Zero Mass Gain (ZMG)	Δ CTE α_{alloy}-$\alpha_{Al_2O_3}$ at 1150°C	Alloy RE Content (at.%)	Alloy Phases at 1150°C*
Ni50Al+Hf	>1000	5.8	0.05 Hf	
NiPt52Al+Hf	>1000	5.0	0.05 Hf	
NiPt50Al+Hf	>1000	6.0	0.05 Hf	
NiPt52Al	>1000	5.1	None	
René N5	~1000	7.1	0.003Y 0.05 Hf	+ '
Ni25Al+Hf	830	5.5	0.06 Hf	'
Ni7Cr13Al+Y	~675	9.2	0.12 Y	
NiPt-39Al	~400	6.0	None	
Ni10Cr19Al+Y	~325	7.7	0.04 Y	+ '
Ni-50Al	~220	5.7	None	
NiCoCrAl+Y	~175	9.0	0.032 Y	n.d.
Ni20Cr19Al+Y	~120	10.2	0.05 Y	+
Ni40Al	~40	5.9	None	

* NiCrAl phase compositions based on Ref. 35.
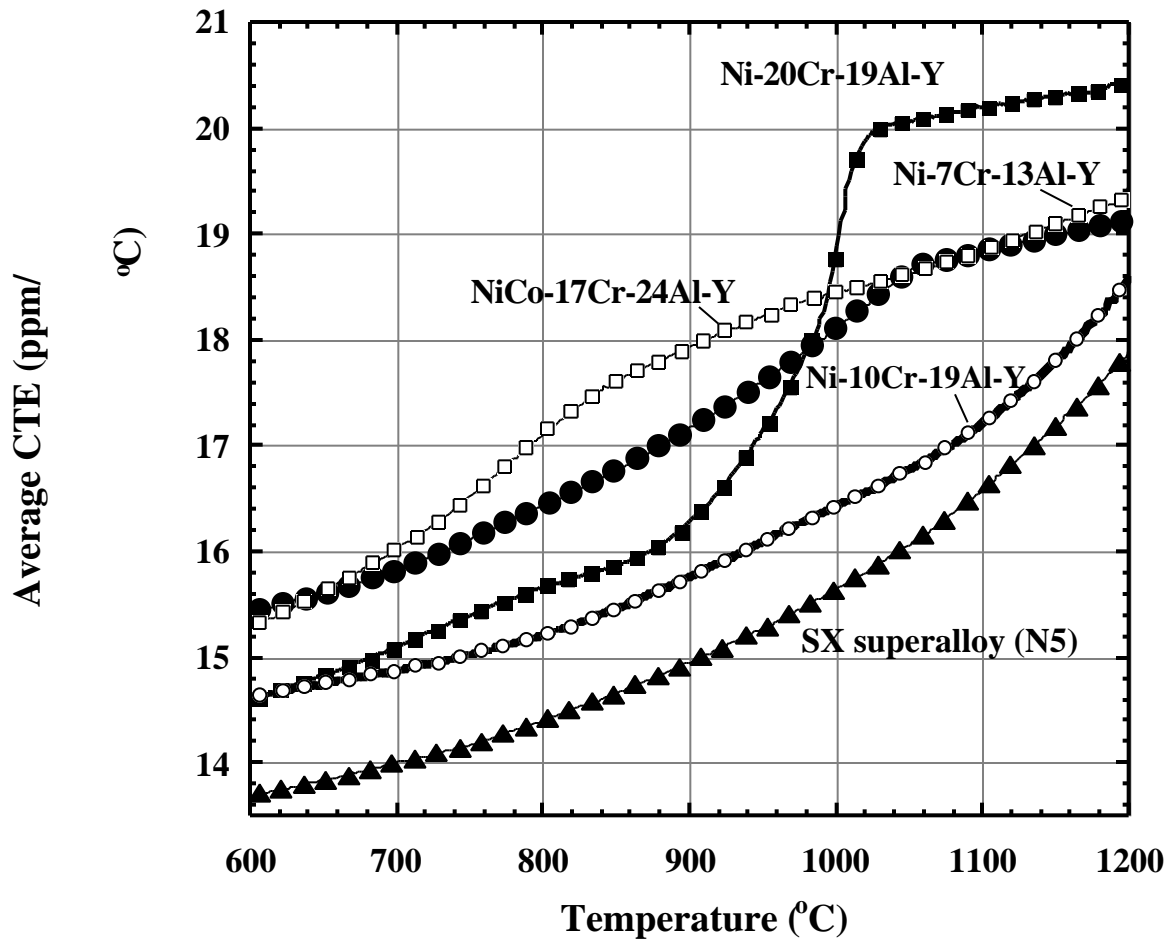
Figure 1. Plots comparing the higher-temperature regions of the average CTE curves for cast NiCrAlY alloys and a single-crystal Ni-base superalloy.
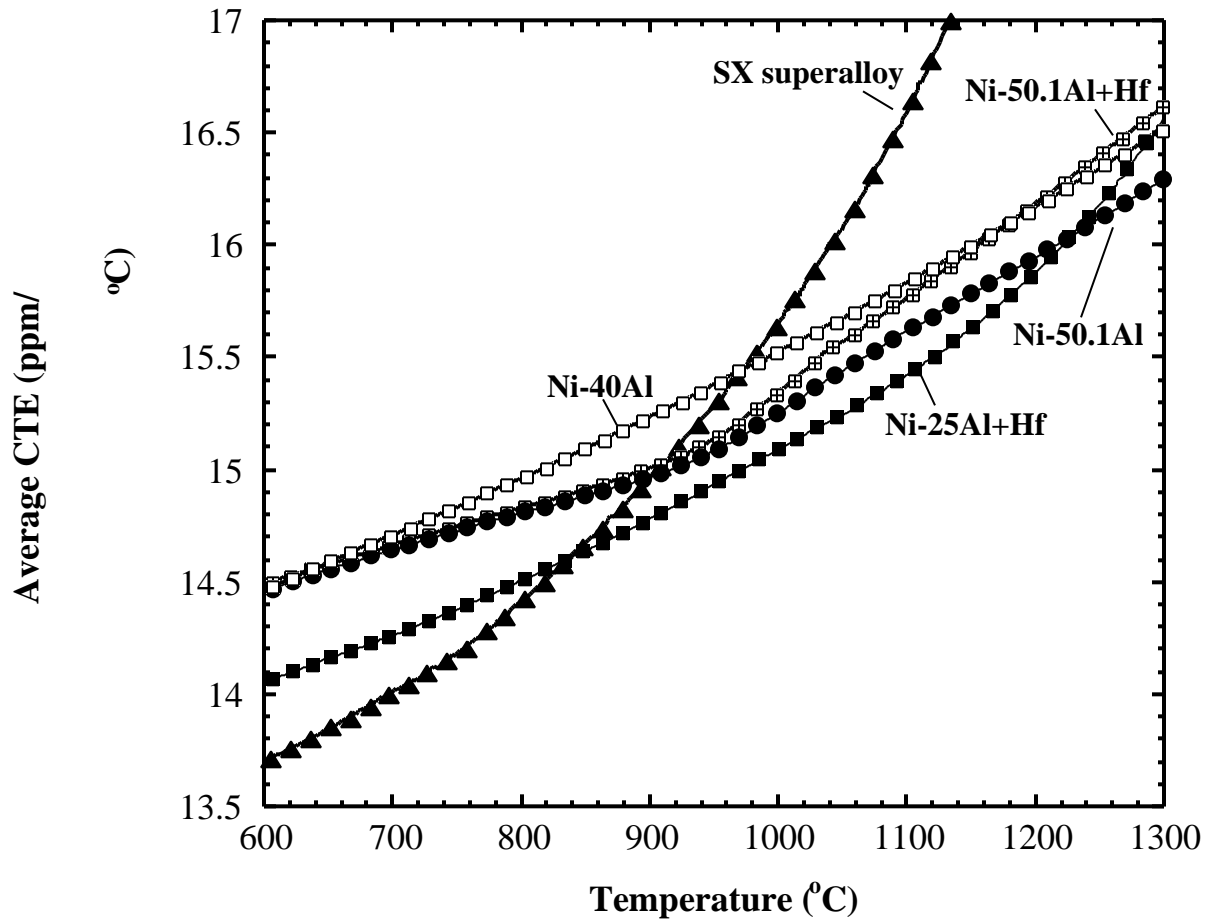
Figure 2. Plots comparing the higher-temperature regions of the average CTE curves for cast NiAl, Ni$_3$Al and a single-crystal Ni-base superalloy.
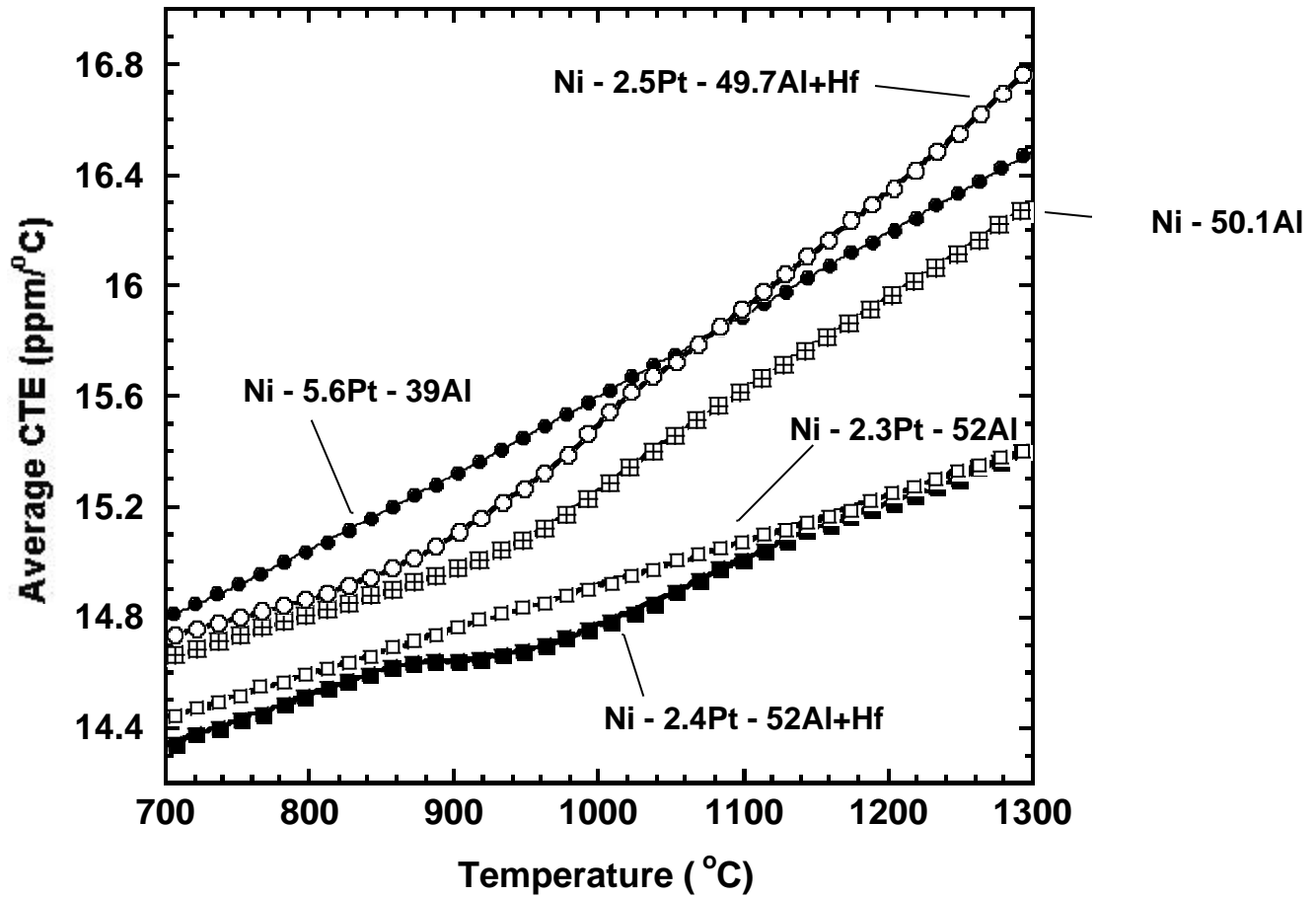
Figure 3. Plots comparing the higher-temperature regions of the average CTE curves for cast (Ni,Pt)Al, and NiAl. The hyperstoichiometric Pt-modified aluminides exhibited a remarkably lower average CTE at temperatures above 950°C.
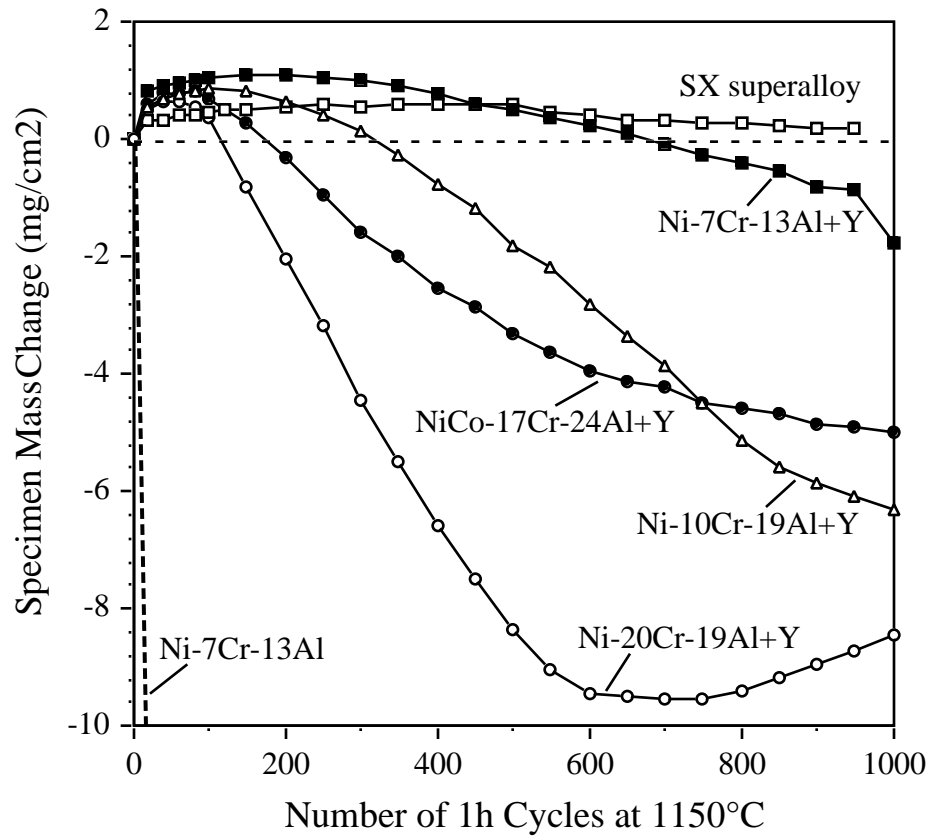
Figure 4. Cyclic oxidation performance of cast NiCrAl and the single-crystal Ni-base superalloy during 1h cyclic testing at 1150°C. Note the important benefit of Y on scale adherence to Ni-7Cr-13Al.
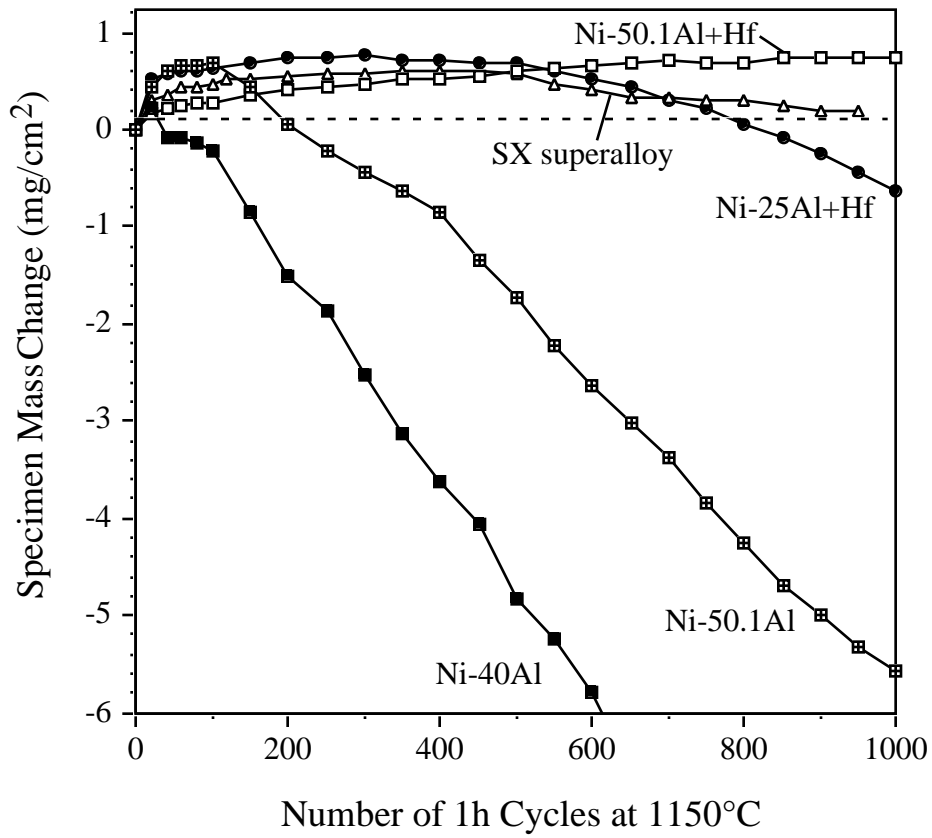
Figure 5. Cyclic oxidation performance of cast NiAl, Ni$_3$Al and a single-crystal Ni-base superalloy during 1h cyclic testing at 1150°C. Note the beneficial effect of Hf on scale adherence to Ni-50.1Al.
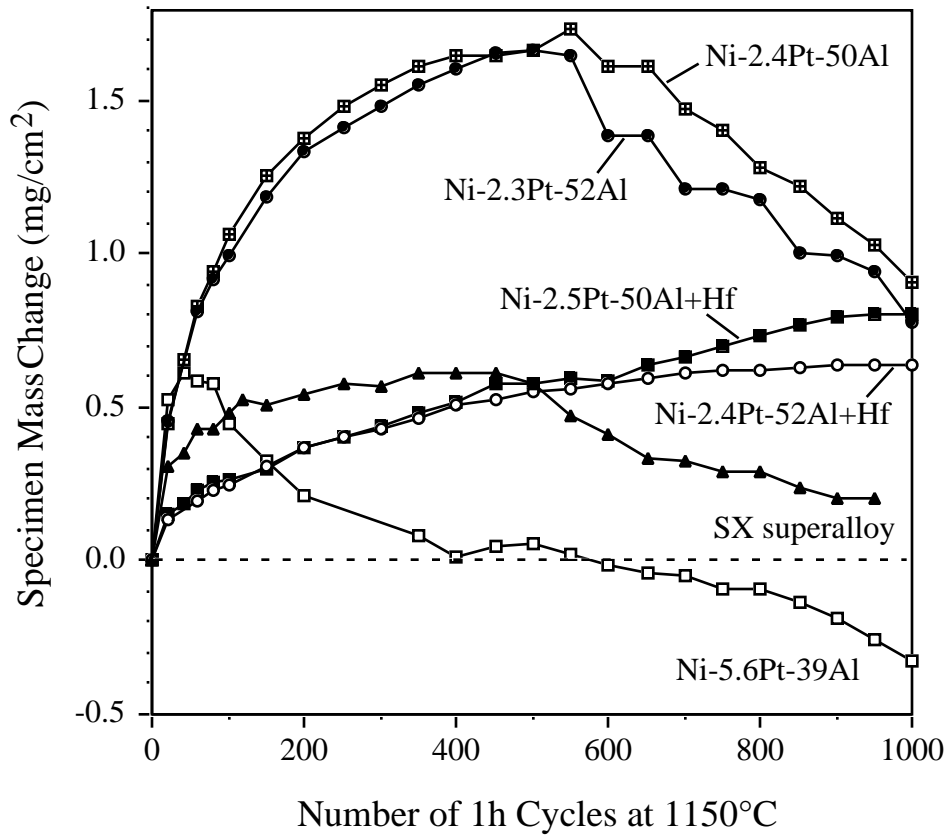
Figure 6. Cyclic oxidation performance of SX superalloy and cast (Ni,Pt)Al alloys during 1h cyclic testing at 1150°C. The addition of Pt improved scale adherence, but not to as great an extent as Hf. Note that NiPtAl with 50 and 52% Al showed near identical oxidation behavior.
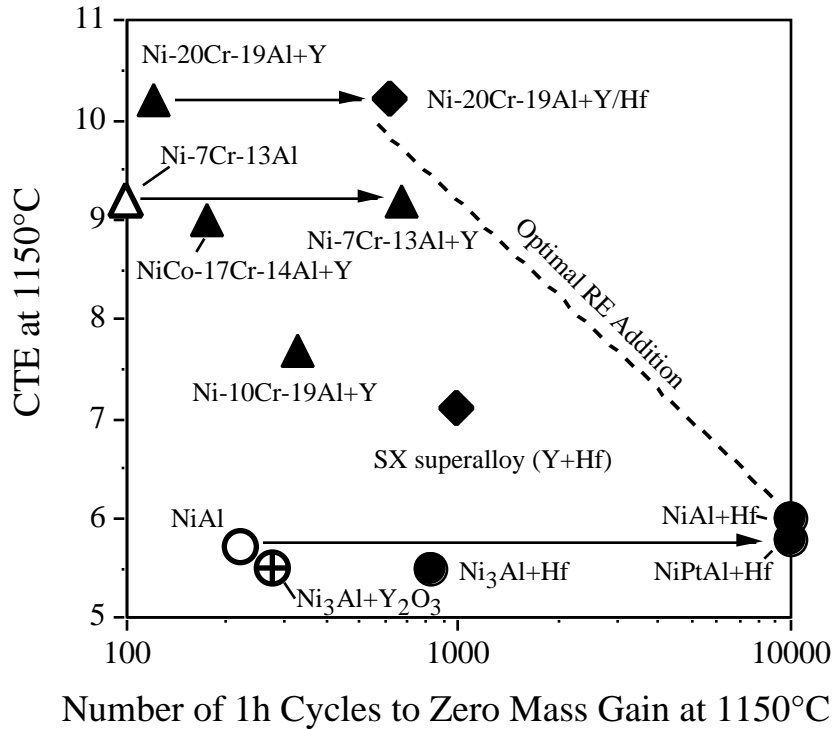
Figure 7. Plot of thermal expansion difference between the alloys and alumina versus spallation resistance at 1150°C. Spallation resistance is expressed as a function of the number of 1-h cycles to zero mass gain for a 1.5mm thick specimen during testing at 1150°C. Additional alloys are included to illustrate the role of RE additions (e.g. Y,Hf) and alloy strength on performance. Arrows illustrate the change in spallation resistance for similar base alloys after addition or optimization of a RE addition.